Efficient Thermal Simulation of Power Modules using Proper Orthogonal Decomposition

Z. Bosnjic^{1*}, F. Koenigseder² and M. Hartmann¹

1 Electric Drives and Power Electronic Systems Institute (EALS), Graz University of Technology, Graz, Austria

2 Magna Power Train GmbH, Traiskirchen, Austria

*E-mail: zlatko.bosnjic@tugraz.at

Abstract—Accurate thermal simulation of power semiconductor modules often relies on the Finite Element Method (FEM) which is time consuming due to the high system order caused by the structure of the module. In this work the applicability of Proper Orthogonal Decomposition (POD) method for reduced order thermal modeling and simulation of power modules is analyzed in detail. By applying this method, system order can be reduced considerably without losing accuracy. A typical half-bridge power module arrangement is used for the study and 3D static as well as 3D transient simulation results show that simulation speed can be increased significantly by applying this approach. Additionally, a comprehensive sensitivity analysis confirms the robustness of the approach with respect to the selection of POD modes according to their energy content.

Index Terms—Thermal simulation, Reduced Order Modeling, Proper Orthogonal Decomposition (POD), IGBT Power Module

I. INTRODUCTION

Performance of power converters is advancing rapidly, driven by a growing demand for efficient power conversion. Modern converters must achieve both high efficiency and high power density while operating at increasing switching frequencies and generating high power loss densities. As a result, the power semiconductor switches of the converter are designed to operate near their temperature limits $T_{i,max}$ without exceeding them $(T_j < T_{j,max})$. It is, therefore, essential to accurately predict power semiconductor junction temperature profiles at different steady state and transient operating points during converter design. Power semiconductor temperatures are usually estimated either by employing detailed numerical simulation methods, such as the Finite Element Method (FEM) and the Finite Difference Method (FDM), which can be computationally intensive, or by means of lumped thermal networks in Foster or Cauer representation. These representations, however, are approximations that do not describe the temperature field inside of the power module and lack accuracy [1].

This paper proposes the application of a Reduced Order Modeling (ROM) method for computationally efficient and accurate thermal simulation of power modules and outlines the advantages and drawbacks of the Proper Orthogonal Decomposition (POD) method. A significant increase in simulation speed (multiple orders of magnitude) is observed when obtaining simulation results by means of POD when compared to FEM simulation while sacrificing some accuracy. Although

POD method has been used in different fields of engineering for over a century [2], it's usefulness is lately becoming more obvious in the field of thermal simulation as the complexity of FEM thermal models is increasing [3], [4]. Proper Orthogonal Decomposition is a well studied numerical method used for decomposition of physical fields $u(\mathbf{x},t)$ into it's singular value components. The method is tightly linked to Singular Value Decomposition (SVD) and Principal Component Analysis (PCA) [3], [5] and [6].

The POD method has already been used in power electronics and more details can be found in [5] and [7]. In [5], POD has been applied to power electronic converters, however no analysis on the effects of model order on accuracy and simulation speed is discussed. In [7], the applicability of the POD method is shown for thermal simulations of a discrete MOSFET switch. In this work the applicability of the POD method in semiconductor power modules in terms of simulation speed and accuracy is analyzed in detail and the effects of reduced model order by the POD method on simulation accuracy is studied and discussed. The POD method is thereto applied on a commercially available semiconductor power module for automotive applications. In Section II an overview on the POD methodology is given including the main steps of the process and in **Section III** the application of the method on the semiconductor power module is shown including comprehensive simulation results. Next, in Section IV, the influence of model order on simulation speed and accuracy is analyzed. Finally a conclusion summarizes the main aspects in Section V.

II. POD METHODOLOGY

For the description of the basic approach of POD, it is assumed that the temperature field $T(\mathbf{x},t)$ has been determined, e.g. as a result of a comprehensive FEM simulation. By applying POD to a thermal problem, this solution temperature field

$$T(\mathbf{x},t) = \sum_{i=1}^{n} \phi_i(\mathbf{x}) \, a_i(t) \approx \sum_{i=1}^{r} \phi_i(\mathbf{x}) \, a_i(t) \tag{1}$$

is decomposed into n singular values without a loss of accuracy [2]. In (1), $\phi_i(\mathbf{x})$ is the i-th component of the orthogonal spatial POD basis functions, $a_i(t)$ is the i-th projection vector in the basis space and n is the order of the system. The singular values are subsequently ordered by energy content

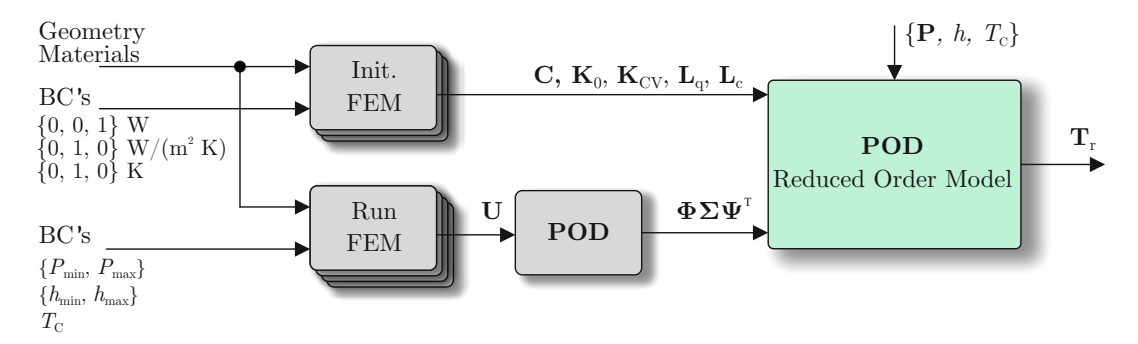


Fig. 1: Block diagram representation of POD method.

and it's possible to extract $r \ll n$ first singular values, called modes. Dependent on the number of selected modes r, model accuracy is reduced to a greater or lesser extent. POD can also advantageously be expressed in matrix form

$$\mathbf{T} = \mathbf{\Phi} \, \mathbf{a}(t) \approx \mathbf{\Phi}_r \, \mathbf{a}_r(t). \tag{2}$$

A key benefit of POD is the possibility to reuse the generated reduced order model for different operating points (boundary conditions) of the thermal problem by calculating the projection vector \mathbf{a}_r in the reduced order space $\mathbf{\Phi}_r$. Dependent on r this increases computation speed considerably, as the order of the system is reduced from n to r. Once the reduced order model has been extracted there is no need for (commercial) FEM software to solve the thermal problem which is another benefit of POD. In Fig. 1, the workflow for POD extraction is outlined and the individual steps will be discussed below. Detailed mathematical derivation of POD can be found in [2], [3] and [8]. In the next section, the applicability of POD for thermal simulation of a commercial power module is analyzed. The results, as well as accuracy and simulation speed comparison, are presented for static 2D and 3D simulations as well as transient 3D simulation.

A. Model Setup for Power Module Simulation

In order to derive a POD model for transient thermal simulation of power modules, this paper assumes a FEM model as the starting point. The workflow for the derivation of POD models from FEM simulation is depicted in Fig. 1. The FEM model is defined by geometry, material properties and boundary conditions (BC's). Geometry of the power module is given by the manufacturing and it is assumed that the geometry of the power module doesn't change during operation, e.g. as a result of higher temperatures. Thermal expansion is therefore not considered in the thermal model due to the very small changes in the thermal behavior, however, thermal expansion is a very important aspect if reliability is in the focus. Although standard materials used in state-of-the-art power modules (such as copper, silicon, solder, ceramic) exhibit some temperature dependence in their properties, this variation is relatively small over the expected temperature range [9] and is therefore neglected in further analysis. Boundary conditions imposed on the power module are defined by the operating

point of the converter. The operating point, and in turn the boundary conditions are given by semiconductor power losses $\{p_{T1+}(t), p_{D1+}(t), p_{T1-}(t), p_{D1-}(t)\}$ and the cooling system. Here, it is assumed that the power semiconductor losses are averaged over one switching period and consist of conduction power losses $p_{\rm c}(t)$ and switching power losses $p_{\rm sw}(t)$

$$p(t) = p_{\rm c}(t) + p_{\rm sw}(t)$$
 (3)

The instantaneous, over one switching period averaged, conduction power losses are then calculated by

$$p_{c}(t) = i_{on}(t) v_{on}(t) d(t)$$

$$\tag{4}$$

where $i_{on}(t)$ is the current through the semiconductor during the on-time period, $v_{\rm on}(t)$ is the on-state voltage drop of the power semiconductor switch and d(t) is the corresponding duty cycle. The instantaneous switching losses are given by

$$p_{\rm sw}(t) = \left[E_{\rm on}(t) + E_{\rm off}(t) \right] f_{\rm sw}. \tag{5}$$

where $E_{\rm on}(t)$ and $E_{\rm off}(t)$ are the turn-on and turn-off switching losses, respectively and $f_{\rm sw}$ is the converter switching frequency. For the cooling system of the power module (forced) heat convection is assumed and the coolant temperature T_c , coolant flow rate $\dot{Q}_{\rm c}$ along with coolant fluid (e.g. air, water, water-glycol mix) properties define the boundary conditions. Please note that inside the power module heat conduction occurs and that heat radiation has been neglected so that on the boundaries of the module only heat convection occurs. Using these conditions the coefficient of heat convection of the power module

$$h = f(\rho, c, T_c, \dot{Q}_c). \tag{6}$$

is defined which shows values in the range of 100 to $800~\mathrm{W/(m^2\,K)}$ for forced air cooling and $1000~\mathrm{to}~10000$ W/(m² K) for liquid cooling depending on cooling system design and materials [10]. For FEM simulation, boundary conditions need to be defined and the following types are commonly used:

- Fixed temperature $T=T_0$ on the boundary $\Gamma_{\rm d}$
- (Dirichlet Type BC)
 Fixed heat flux $\frac{dT}{dn} = q_0$ through the boundary Γ_n (Neumann Type BC)

• Fixed convection rate $aT + b\frac{dT}{dn} = g$ at boundary $\Gamma_{\rm r}$ (Robin Type BC).

Dirichlet Type BCs are rarely used in thermal modeling of power electronics. The Neumann Type BC is used for modeling of heat sources such as semiconductor power losses and thermally insulated regions of the module while the Robin Type BC is used to model the convective heat transfer of the heat sink connected to the power module.

Assuming homogeneous, isotropic, as well as temperatureindependent material parameters in the individual layers of the power module stack, the governing equation of a thermal FEM model is

$$\mathbf{C}\frac{d\mathbf{T}(t)}{dt} + \mathbf{K}\mathbf{T}(t) = \mathbf{L} \tag{7}$$

where ${\bf C}$ is the heat capacitance matrix in $W\,s/K$, ${\bf K}$ is the heat conductance matrix in W/K, ${\bf L}$ is the load vector in W and ${\bf T}$ is the vector of resultant nodal temperatures in K. Matrices ${\bf C}$ and ${\bf K}$ define the heat capacitance and heat conductance between mesh nodes, respectively. The load vector ${\bf L}$ describes the boundary conditions imposed on the model. These matrices and vectors are extracted from FEM simulation software and are later used for assembling the POD model.

The heat capacitance matrix \mathbf{C} is defined by geometry and material properties and is independent of the boundary conditions. This matrix is extracted from FEM simulation software after the geometry and materials have been defined without the need to perform a FEM simulation. For Dirichlet Type and Neumann Type BCs, the heat conductance matrix \mathbf{K} is not dependent on the values assigned to the boundaries Γ_d or Γ_n . However, for Robin Type BCs, the value of the edge elements of \mathbf{K} are dependent on the BC value. Therefore, the matrix \mathbf{K} is split into a constant part and a part dependent on heat convection h

$$\mathbf{K}(h) = \mathbf{K}_0 + h\mathbf{K}_c \tag{8}$$

where \mathbf{K}_0 and \mathbf{K}_c are both independent of boundary conditions and can again be extracted without running a FEM simulation. The load vector \mathbf{L} depends on the boundary conditions

$$\mathbf{L} = \mathbf{P}^{\mathrm{T}} \mathbf{L}_{\alpha} + h T_{c} \mathbf{L}_{c}. \tag{9}$$

where ${\bf P}$ is the vector of heat sources, e.g. given by the semiconductor power losses (3) to (5). Temperature $T_{\rm c}$ is the coolant temperature. The load vector ${\bf L}$ is therefore split into a heat source dependent part ${\bf L}_{\rm q}$ and a part defining the convection ${\bf L}_{\rm c}$ to coolant.

In a next step the two vectors $\mathbf{L_q}$ and $\mathbf{L_c}$ need to be determined by a simple procedure. First, all heat sources are set to zero $\mathbf{P} = \vec{0}\,\mathrm{W}$ and heat convection is set to $h = 1\,\mathrm{W/(m^2\,K)}$. By simulating this simple arrangement, the vector $\mathbf{L_q}$ can be extracted. Then by setting $\mathbf{P} = 1\,\mathrm{W}, \, h = 0\,\mathrm{W/(m^2\,K)}$ and $T_\mathrm{C} = 0\,\mathrm{K}$, the vector $\mathbf{L_c}$ can be recovered. Substituting (8) and (9) into (7) a suitable form for (7) is obtained for POD simulation

$$\mathbf{C}\frac{d\mathbf{T}(t)}{dt} + (\mathbf{K}_0 + h\,\mathbf{K}_c)\,\mathbf{T}(t) = \mathbf{P}^{\mathrm{T}}\,\mathbf{L}_{\mathrm{q}} + h\,T_{\mathrm{c}}\,\mathbf{L}_{\mathrm{c}}.$$
 (10)

It should be noted that by setting $\frac{d\mathbf{T}(t)}{dt} = 0$, the system of equations in (10) reduces to

$$(\mathbf{K}_0 + h\,\mathbf{K}_c)\,\mathbf{T} = \mathbf{P}^{\mathrm{T}}\,\mathbf{L}_0 + h\,T_c\,\mathbf{L}_c \tag{11}$$

which is the steady-state form of the FEM thermal problem. Equation (10) or (11) can now be solved for an arbitrary converter operating point without the need for FEM software using numerical ODE solvers (e.g. using MATLAB, OCTAVE, Python, ...).

B. Solution Snapshot Matrix

For application of the POD approach, a solution snapshot matrix is required. Solution vectors \mathbf{T}_i are thereto calculated for boundary conditions that define the corner cases of converter operation. These solutions are subsequently used to form a snapshot matrix

$$\mathbf{U} = [\mathbf{T}_1 \ \mathbf{T}_2 \ \dots \ \mathbf{T}_n] \,. \tag{12}$$

A three-phase two-level topology based on IGBT technology is used in this work. The basic topology as well as the structure of the power module is depicted in **Fig. 2**. It should be noted that only a half-bridge leg of a power module is analyzed, as thermal coupling between semiconductor dies of adjacent bridge legs in a two-level three-phase power module are very small and can be neglected. The operating points of interest are shown in **Fig. 3** and span the full operating range of the converter where $P_{\rm x} \in \{P_{\rm T1+}, P_{\rm D1+}, P_{\rm T1-}, P_{\rm D1-}\}$. Considering the operating points shown in **Fig. 3** for the half-bridge layout shown in **Fig. 2**, in total n=16 solutions are obtained.

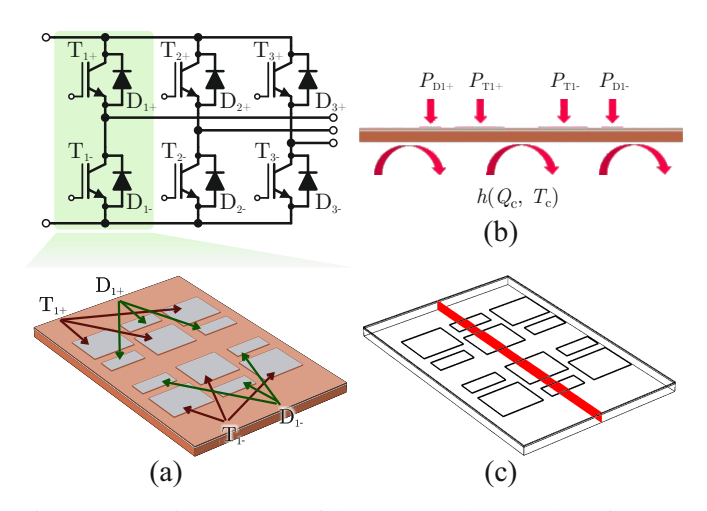


Fig. 2: (a) Basic structure of the two-level three-phase inverter topology based on IGBT technology and indicated half-bridge geometry of the power module with three IGBT chips and three diode chips in parallel, (b) 2D cross section of the power module with indicated boundary conditions and (c) wire-frame geometry of the half-bridge with indicated cross section.

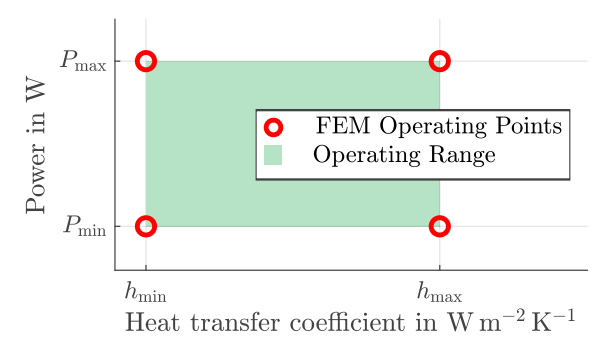


Fig. 3: Corner case operating points of the half-bridge used for assembly of the snapshots matrix with indicated operating range of the half-bridge.

Finally, Proper Orthogonal Decomposition (POD) on the snapshot matrix is preformed to obtain

$$\mathbf{U} = \mathbf{\Phi} \, \mathbf{\Sigma} \, \mathbf{\Psi}^{\mathrm{T}} = \sum_{i=1}^{m} \sigma_i \, \boldsymbol{\phi}_i \, \boldsymbol{\psi}_i^T$$
 (13)

where Φ is the POD basis matrix, Σ is a diagonal matrix containing the singular values of the snapshot matrix and Ψ is orthogonal to Φ . Derivation of (13) is omitted here and can be found in [2]. The basis matrix Φ contains all the spatial information of the snapshot matrix U and can be used to fully reconstruct the solutions $\{T_1, T_2, ..., T_n\}$ by substituting (2) into (10)

$$\mathbf{C}\frac{d\mathbf{\Phi} a(t)}{dt} + (\mathbf{K}_0 + h\,\mathbf{K}_c)\,\mathbf{\Phi} a(t) = \mathbf{P}^{\mathrm{T}}\,\mathbf{L}_{\mathrm{q}} + h\,T_c\,\mathbf{L}_{\mathrm{c}} \quad (14)$$

and solving for a(t). The real advantage of POD is, however, that a reduced basis Φ_r with order r << m is chosen. The resulting system of equations

$$\mathbf{C}\frac{d\mathbf{\Phi}_{r} a_{r}(t)}{dt} + (\mathbf{K}_{0} + h \,\mathbf{K}_{c}) \,\mathbf{\Phi}_{r} a_{r}(t) = \mathbf{P}^{T} \,\mathbf{L}_{q} + h \,T_{c} \,\mathbf{L}_{c}$$
(15)

is computationally much easier to solve due to considerably reduced system order. Selection of the number of POD modes r is based on relative energy content $\epsilon(r)$ of the reduced order model

$$\epsilon(r) = \frac{\sum_{i=1}^{r} \sigma_i}{\sum_{i=1}^{n} \sigma_i}$$
 (16)

where σ_i is the i-th diagonal element of the singular value matrix Σ in (13). Usually, the relative energy content given in (16) is determined heuristically. The number of POD

TABLE I: Half-bridge geometry data.

Component	Dimensions			
Component	X	у	Z	
IGBT	10.0 mm	9.2 mm	120 µm	
Diode	$9.8~\mathrm{mm}$	5.1 mm	$120~\mu\mathrm{m}$	
Top Copper	70 mm	43 mm	310 µm	
Alumina	$70~\mathrm{mm}$	$43~\mathrm{mm}$	$380~\mu\mathrm{m}$	
Bottom Copper	$70~\mathrm{mm}$	$43~\mathrm{mm}$	$2~\mathrm{mm}$	

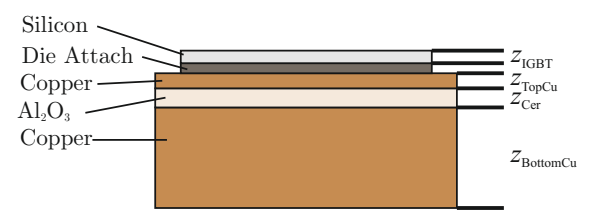


Fig. 4: Half-bridge cross section with indicated materials and thicknesses.

modes r defines the order of the system given in (15) and, in turn, defines the accuracy and simulation speed of the reduced order model. Proper selection of used POD modes r is therefore essential for good accuracy while considerably reducing simulation speed. In **Section IV**, the effects of model order on simulation speed and accuracy are therefore analyzed in detail.

III. APPLICATION OF POD TO POWER MODULES

After deriving the framework needed for POD thermal simulation in Section II, POD reduced order modeling is applied on the half-bridge depicted in Fig. 2 and presented in this section. The analyzed half-bridge is based on a bridge leg of a commercially available three-phase power module with a rated voltage of 750 V and a rated current of 660 A (Infineon FS660R08A6P2FLB [11]). The half-bridge contains three paralleled IGBT semiconductor dies as well as three paralleled diode dies per switch. For thermal modeling of the power module the geometry data is needed and the corresponding geometry data of the half-bridge leg is given in Table I. The full half-bridge power module shows the size $70 \,\mathrm{mm} \,\mathrm{x} \,43 \,\mathrm{mm}$ and a thickness of $2.3 \,\mathrm{mm}$ consisting of an alumina-based Direct Bonded Copper (DBC) substrate with copper layers on top and bottom of the ceramic. The dies are soldered to the top copper layer and corresponding thicknesses of the die attach layer as well as IGBT and diode dies are estimated and summarized in Table I. Corresponding material properties of the power module are estimated as well and are given in Table II. As stated in the previous section, for POD thermal modeling, material properties are assumed to be temperature independent as the relative change in the target operating range is low (< 5%). In the following the applicability, accuracy and speed of the POD ROM approach is analyzed using 2D steady-state simulation, 3D steady-state as well as 3D transient simulations.

TABLE II: Material properties of the IGBT half-bridge.

Material	Density ρ	Thermal cond. σ	Specific heat $c_{ m p}$
	in ${\rm kg/m^3}$	in $W/(m K)$	in $J/(kg K)$
Silicon	2330	130	700
Die Attach	7370	48	180
Copper	8800	400	385
Alumina	3900	27	900

A. 2D Static Results

For validation of the POD reduced order model approach in 2D static case, a cross section of the half-bridge depicted in Fig. 2 is taken as the reference geometry (cf., Table I). Temperature distribution on this domain is calculated both with FEM and POD ROM for a steady-state operating point and simulation results are compared in order to verify the accuracy of POD. The IGBTs T_{1+} are thereto modeled with losses of $P_{\rm v}=72\,\rm W$ which corresponds to a current of $I_{\rm c}=120\,\rm A$ and an on-state voltage drop of $V_{\rm ce,on}=0.6\,\rm V$. All other IGBTs and diodes don't show power losses. A coolant temperature of $T_{\rm C}$ of 65 °C and a heat convection coefficient of $h=1500\,\rm W/(m^2\,\rm K)$ is used as operating point for the cooling system.

Based on the theoretical derivation outlined in **Section II**, a 2D POD model is here derived for steady-state simulation of the half-bridge cross section shown in **Fig. 2a**. Firstly, the half-bridge cross section geometry (**Table I**) is modeled in FEM software and the corresponding material properties (**Table II**) are applied to simulation domains. Next, the simulation domain is meshed and heat conductance matrices \mathbf{K}_0 and \mathbf{K}_c are extracted. Finally, load vectors, \mathbf{L}_q and \mathbf{L}_c are extracted by performing the required FEM simulations as described in **Section II** and a matrix equation in the form of (11) is obtained. A snapshots matrix \mathbf{U} , with four FEM solutions, is formed by setting $h_{\min} = 1 \ \mathrm{W}/(\mathrm{m}^2 \ \mathrm{K}), \ h_{\max} = 2000 \ \mathrm{W}/(\mathrm{m}^2 \ \mathrm{K}), \ P_{\min} = 1 \ \mathrm{W}$ and $P_{\max} = 80 \ \mathrm{W}$. The operating points selected for generation of the snapshots matrix represent the full expected converter operating range. POD is then

applied to the snapshots matrix U in order to obtain the basis matrix Φ and singular value matrix Σ which can now be used for reduced order modeling.

Due to thin material layers in the half-bridge structure, a fine mesh with m=8968 mesh nodes is required for 2D FEM simulation. On the other hand, simple geometry of the half-bridge module allows for a large reduction in the model order when using POD. Setting $\epsilon(r)>99\%$ in (16), a value of r=4 is obtained. This corresponds to a reduction of model order by a factor of 2242. In **Fig. 5 a** the temperature distribution plot of the obtained POD simulation is given and in **Fig. 5 b** the error compared to FEM simulation results is shown. The obtained results are in good agreement, even if only 4 POD modes have been selected. A maximal absolute error of $\max |T_{\rm POD}-T_{\rm FEM}|=0.17^{\circ}\,{\rm C}$ is achieved between FEM and POD simulation which is well within the expected accuracy of FEM thermal simulations for power modules.

B. 3D Static Results

Similar to the 2D case, also for the 3D static case FEM simulations of the 3D half-bridge geometry shown in **Fig. 2** have been performed and a reduced order model has been derived based on the POD approach. Same load points and cooling condition as for the 2D static simulation have been considered and the same derivation steps are applied. Both models, the full FEM model as well as the POD model are simulated and corresponding simulation results are shown in **Fig. 6**. The required FEM mesh for the 3D half-bridge geometry is rather fine and contains $m=1\,286\,450$ nodes. Assuming the same relative energy content criterion $(\epsilon(r)>99\%)$ as for the 2D

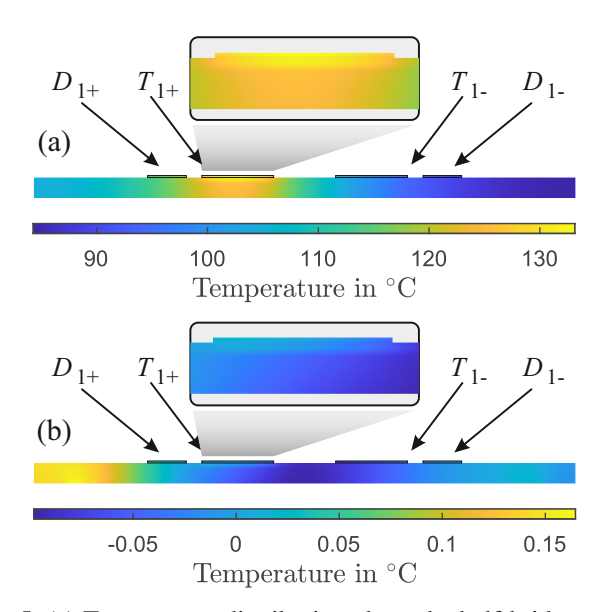


Fig. 5: (a) Temperature distribution along the half-bridge cross section with 72 W of IGBT T_{1+} power loss and h=1500 W/(m² K) simulated using POD reduced order model with r=4 modes, and (b) Simulation error between POD reduced order model and Finite Element Method with m=8968 mesh nodes.

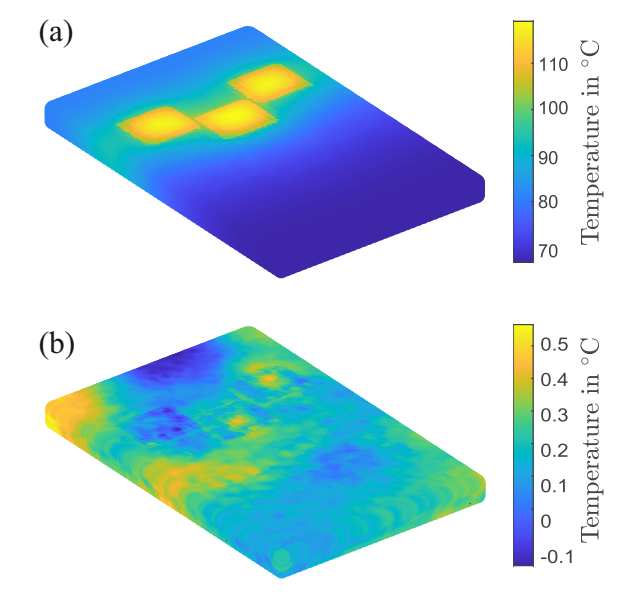


Fig. 6: (a) Temperature distribution on surface of the half-bridge with 72 W of IGBT T_{1+} power loss and $h=1500\,\mathrm{W/(m^2\,K)}$ simulated using POD reduced order model with r=2280 modes, and (b) Simulation error between POD reduced order model and Finite Element Method with $m=1286\,450$ mesh nodes.

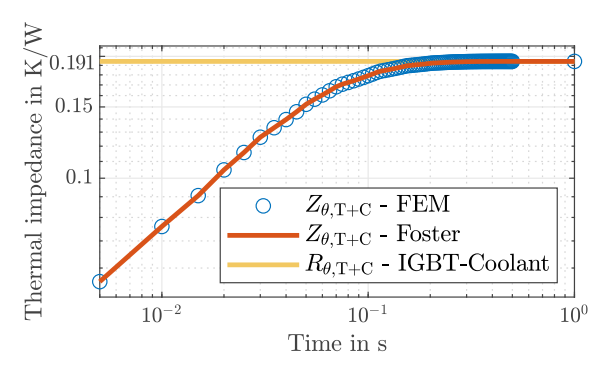


Fig. 7: Transient thermal impedance of the IGBT die $Z_{\theta T+C}$ extracted from FEM simulation along with Foster representation and indicated steady-state thermal resistance $R_{\theta T+C}$.

case, a model order of r=2280 is obtained. This corresponds to a model order reduction of 564 times. Similar to the 2D static case the simulated results are in good agreement and a maximal absolute error of $\max |T_{\rm POD} - T_{\rm FEM}| = 0.72$ °C is achieved between FEM and POD.

C. 3D Transient Results

Derivation of the 3D POD reduced order model for transient thermal simulation of the half-bridge given in Fig. 2 a is based on the steps presented in Section II starting with geometry and material definitions in FEM software. Unlike the static cases, the equation system describing the transient thermal behavior is time dependent as shown in (10). Therefore, the heat capacitance matrix C needs to be extracted from FEM software next to the heat conductance matrices. In addition, the load vectors \mathbf{L}_{q} and \mathbf{L}_{cv} are obtained by applying the boundary conditions defined in Section II. The snapshots matrix Uthat defines the edge-case operating conditions of the halfbridge is extracted from FEM software by simulating the operating points depicted in Fig. 3. It should be noted that the semiconductor powers $\{P_{T1+}, P_{D1+}, P_{T1-}, P_{D1-}\}$ are time dependent for the transient simulation case. For accurate calibration of the transient POD ROM, the semiconductor power losses are applied as step functions

$$P(t) = P u(t - \tau) \tag{17}$$

where P is the DC power value, u(t) is the unit step function and τ is the time delay of the step, selected to be equal to one simulation time step [5]. Applying POD to the snapshots matrix U, the basis matrix Φ and singular value matrix Σ are obtained which are used for reduced order modeling.

For validation of the accuracy of the POD reduced order model in transient simulations, the junction temperature of a single IGBT chip $T_{i,T1+}(t)$ is taken as reference. In general,

TABLE III: Foster network parameters of the IGBT T_{1+} .

n	1	2	3	4
τ_{θ} , in s	0.0297	0.0183	0.0022	0.0687
$R_{\theta,n}$ in K/W	0.1086	0.0251	0.0393	0.0216

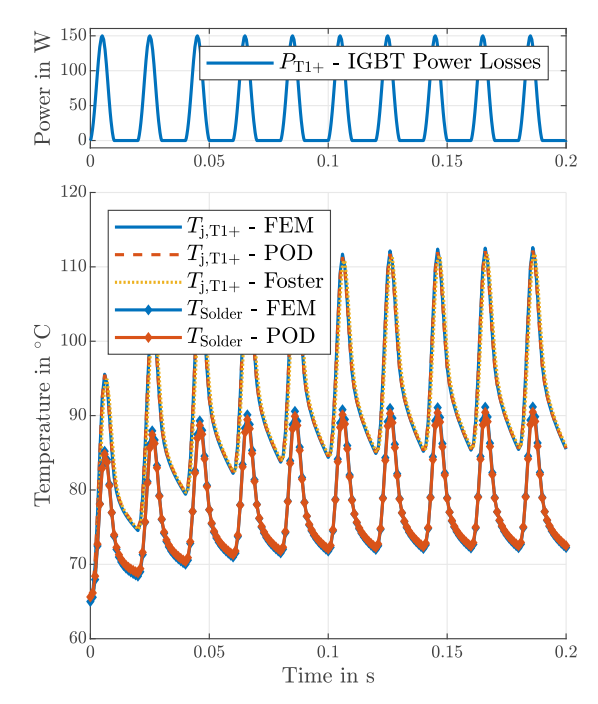


Fig. 8: Simulated power loss profile of the IGBT T_{1+} in half-bridge arrangement when loaded with a sinusoidal output current $I=120\,\mathrm{A}$ and $f=100\,\mathrm{Hz}$ at a DC-link voltage of $400\,\mathrm{V}$ and a switching frequency $f_\mathrm{sw}=10\,\mathrm{kHz}$. Simulated junction temperature using FEM, POD and Foster lumped thermal network along with simulated solder layer temperature using FEM and POD.

the junction temperature of the IGBT chip is not constant over the whole chip area and in this work the temperature in the center of the semiconductor die defines the junction temperature. To be able to better benchmark the achieved results using POD ROM, the results are compared with FEM simulation and further with the results of a simplified Foster lumped network model. The Foster model is derived from FEM simulation by curve-fitting of the transient thermal impedance $Z_{\theta,T+-C}(t)$ to the lumped model (cf., **Fig. 7**). A Foster model with four time constants is used to approximate the thermal behavior and in **Table III** the parameters of the Foster model are given.

Additionally, temperature profiles of the die-attach solder layer are simulated using both the FEM and POD method. The solder layer is selected for comparison, as it is of interest for reliability studies of power modules. Unlike lumped thermal networks, which require a parametrized model for each point of the simulation domain, the POD method directly provides a temperature field distribution in the entire simulation domain. Equivalent ODE solver settings (ODE23tb, $2\,\mathrm{ms}$ step size with relative error of 1e-6) are used for both FEM and POD simulation in order to eliminate the influence of the solver on result accuracy. The converter operating point selected for simulation is assumed to be at peak operating power at highest coolant temperature T_C . The sinusoidal half-bridge

$$i(t) = I\sin(2\pi f t) \tag{18}$$

with an amplitude of $I=120\,\mathrm{A}$ and a frequency of $f=100\,\mathrm{Hz}$ is selected. The converter uses a switching frequency of $f_\mathrm{sw}=10\,\mathrm{kHz}$ and the duty cycle of the half-bridge at this operating point is

$$d(t) = \frac{1}{2} (1 + M \sin(2\pi f t))$$
 (19)

at a modulation index of M=1 and a DC-link voltage of $400\,\mathrm{V}$. Based on (3), (4) and (5) and the operating point parameters, the loss profile is pre-calculated and fed into the FEM simulation model, POD model and Foster network model. Losses are estimated based on power module datasheet [11] and module characterization without accounting for loss temperature dependence.

Comparison of simulated junction temperature profiles, as well as die-attach solder layer temperature profiles is shown in **Fig. 8**. The resulting junction temperature shows an average value of $T_{\rm j,avg}=95.2\,^{\circ}{\rm C}$ and a temperature swing of $\Delta T_{\rm j}\approx30\,^{\circ}{\rm C}$. Both POD and Foster network simulation results show good agreement with results obtained from FEM simulation. The advantage of the POD method is evident in the simulated solder layer temperature profiles. Unlike the Foster model, which provides a result for only a single point in space, the POD simulation generates a full temperature field across the entire simulation domain. Agreement in solder layer temperature profiles depicted in **Fig. 9** validates the accuracy of POD simulation for an arbitrary point of the domain.

IV. SENSITIVITY ANALYSIS

In the previous section, POD-based simulations were conducted using a fixed number of modes r, determined empirically based on the energy content $\epsilon(r)$ of the singular values. However, the selection of r significantly impacts both the accuracy and computational efficiency of the reduced order model (ROM).

This section examines the trade-off between simulation accuracy and computational speed as a function of the number of POD modes (cf., Fig. 9) as well as the influence of the operating point parameters on overall simulation accuracy (see Fig. 10). A FEM simulation serves as the benchmark for assessing the accuracy of POD based ROM. The impact of the number of POD modes on critical performance metrics, including

- Energy content compared to full order model $\epsilon(r)$
- Maximum absolute temperature error compared to FEM simulation $\max |T_{\rm POD} T_{\rm FEM}|$
- Relative speed increase compared to FEM simulation speed $T_{
 m sim,FEM}/T_{
 m sim,POD}$

is evaluated. The results, derived from three-dimensional static thermal simulations of a half-bridge power module, are summarized in **Fig. 9** and illustrate the relationship between model reduction, accuracy, and computational efficiency. The green-shaded regions denote POD models where the absolute

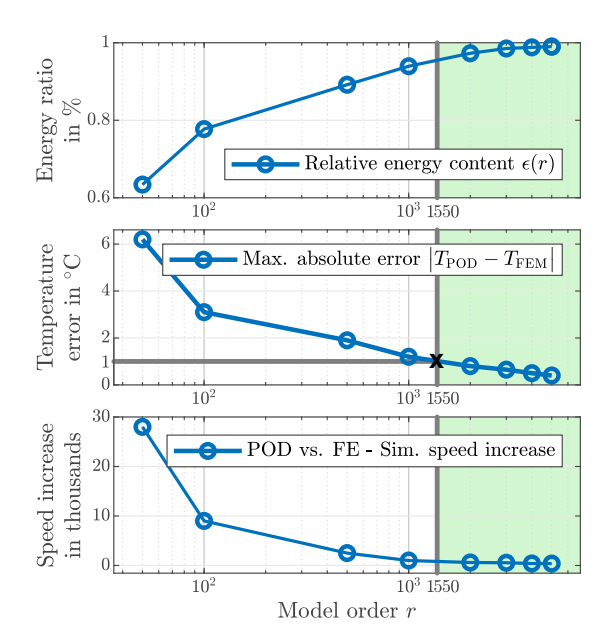


Fig. 9: Energy content, max. absolute error and simulation speed increase as a function of POD model order r.

temperature error remains below one Kelvin compared to the FEM benchmark

$$\max |T_{\text{POD}} - T_{\text{FEM}}| < 1 \,\text{K}. \tag{20}$$

It is interesting to note that POD model order of r=1550 achieves this error threshold while maintaining simulation error below $1\,\mathrm{K}$, as indicated in Fig. 9, which corresponds to a model order reduction by a factor of 830. Additionally, at this model order, 97 % of the energy content of the original model is retained. The simulation speed increase is measured to be 942 at r=1550. The observed simulation speed increase $T_{\mathrm{sim,FEM}}/T_{\mathrm{sim,POD}}$ can vary depending on simulation hardware and software, as well as background computational processes. To reduce the variability caused by background processes, results presented here represent the averaged value of ten independent simulation runs. The variation in the results is especially large for small values of r.

In order to analyze the influence of operating point parameter variation on the POD model accuracy, 3D FEM simulations are run for the full expected operating range of the half-bridge: $P \in [1, 80] \text{ W} \text{ and } h \in [10, 2000] \text{ W}/(\text{m}^2 \text{ K}).$ Simulation results from only four corner cases are then used to obtain the snapshots matrix U and a POD reduced order model is derived based on these corner case results as described in Section II and in **Section III**. Next, thermal simulations are preformed for the full operating range using the POD model derived from the four corner cases with model order r = 3000. Maximum absolute temperature error and maximum relative temperature error are selected as metrics for comparison between FEM and POD. In Fig. 10, the comparison of the FEM and POD results is shown based on simulation accuracy with highlighted operating points used for POD model generation. As can be observed, the maximum absolute error is below 0.75 °C while

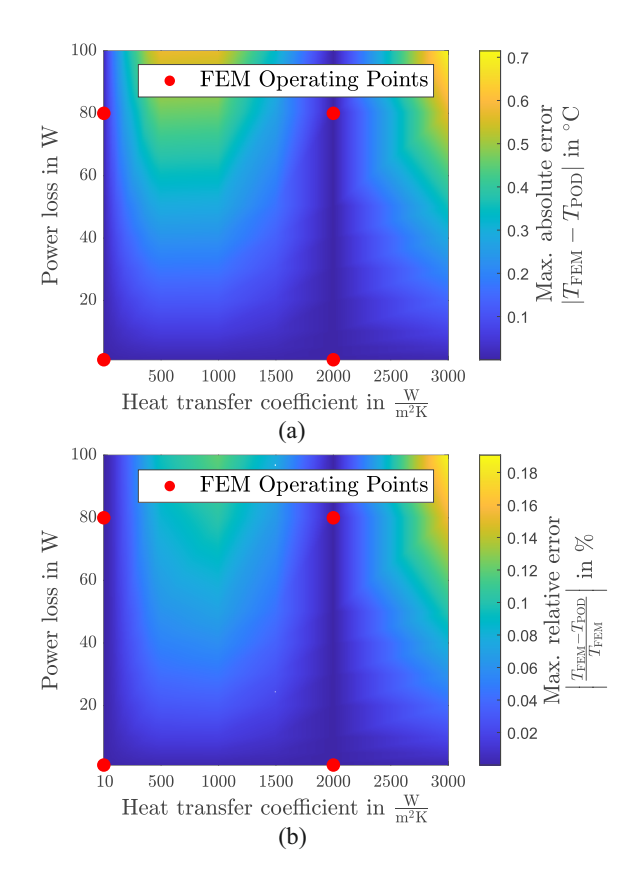


Fig. 10: (a) Maximum absolute temperature error, and (b) Maximum relative temperature error in POD simulation compared with FEM at r=3000 for the full half-bridge operating range $(h \in [10,3000]\,\mathrm{W}/(\mathrm{m}^2\,\mathrm{K}))$ and $P \in [1,80]\,\mathrm{W}$.

the maximum absolute error is below $0.2\,\%$ which validates the usefulness of POD as an alternative to FEM in thermal simulations.

V. CONCLUSION

This paper presented the application of Proper Orthogonal Decomposition (POD) as a Reduced Order Modeling (ROM) technique for computationally efficient thermal simulations of power modules. By leveraging POD, significant speed improvements have been achieved compared to conventional FEM simulations, while maintaining an acceptable level of accuracy. The methodology was validated through 2D and 3D steady-state as well as 3D transient simulations, demonstrating that POD can effectively reduce computational complexity without the need for commercial FEM software for repeated simulations.

Additionally, sensitivity analysis highlighted the trade-offs between model order reduction and accuracy, providing guidelines for selecting an optimal number of POD modes. The results suggest that POD-based ROM can be a viable alternative for thermal simulations in power electronics, particularly in early-stage design iterations where rapid evaluations are necessary. Future work will focus on extending the approach to more complex 3D transient scenarios and a detailed analysis on the effects of module structure on POD effectiveness.

REFERENCES

- [1] A. S. Bahman, K. Ma, and F. Blaabjerg, "A Lumped Thermal Model Including Thermal Coupling and Thermal Boundary Conditions for High-Power IGBT Modules," *IEEE Transactions on Power Electronics*, vol. 33, no. 3, pp. 2518–2530, 2018.
- [2] P. Holmes, J. L. Lumley, and G. Berkooz, *Turbulence, Coherent Structures, Dynamical Systems and Symmetry*. Cambridge University Press, 1996.
- [3] A. Antoranz, A. Ianiro, O. Flores, and M. García-Villalba, "Extended proper orthogonal decomposition of non-homogeneous thermal fields in a turbulent pipe flow," *Int. Journal of Heat and Mass Transfer*, vol. 118, pp. 1264–1275, 2018.
- [4] R. Venters, B. T. Helenbrook, K. Zhang, and M.-C. Cheng, "Proper-Orthogonal-Decomposition Based Thermal Modeling of Semiconductor Structures," *IEEE Transactions on Electron Devices*, vol. 59, no. 11, pp. 2924–2931, 2012.
- [5] H. B. Aissia, "Model reduction for thermal management of high power electronic components for aerospace application," Ph.D. dissertation, Université de Lyon, 2019.
- [6] M. R. Berramdane, A. Battiston, M. Bardi, N. Blet, and B. Remy, "System Identification and Optimization Using ARX Models for Thermal Management in WBG-based Power Electronics Applications," in *Proc. of the 2024 Energy Conversion Congress and Expo Europe (ECCE Europe)*, Darmstadt, Germany, 2024, pp. 1–7.
- [7] Y. Zhao, Z. Wang, D. Luo, C. Chen, B. Ji, and G. Li, "Multitimescale Thermal Network Model of Power Devices Based on POD Algorithm," *IEEE Transactions on Power Electronics*, vol. 39, no. 4, pp. 3906–3924, 2024.
- [8] K. Kunisch and S. Volkwein, "Galerkin proper orthogonal decomposition methods for parabolic problems," *Numerische Mathematik*, vol. 90, pp. 117–148, 2001.
- [9] C. Y. Ho, R. W. Powell, and P. E. Liley, "Thermal Conductivity of the Elements," *Journal of Physical and Chemical Reference Data*, vol. 1, no. 2, pp. 279–421, 1972.
- [10] L. Meysenc, M. Jylhakallio, and P. Barbosa, "Power Electronics Cooling Effectiveness Versus Thermal Iinertia," *IEEE Transactions on Power Electronics*, vol. 20, no. 3, pp. 687–693, 2005.
- [11] HybridPACK Drive Module Datasheet, FS660R08A6P2FLB, Infineon Technologies, 2019. [Online]. Available: https://www.infineon.com/dgdl/Infineon FS660R08A6P2FLB DataSheet v03_00 EN.pdf?fileId=5546d46269e1c019016a793d42f35736.